Gravitational signals underlie tonic muscle activity during goal-directed reaching

Abbreviated title: gravitational motor primitives

Authors and affiliations:

Erienne Olesh[1,3], Bradley Pollard[1,3], and Valeriya Gritsenko[1,2,3,*]

[1] Department of Human Performance, School of Medicine, West Virginia University, Morgantown, West Virginia, United States of America

[2] Department of Mechanical and Aerospace Engineering, Benjamin M. Statler College of Engineering and Mineral Resources, West Virginia University, Morgantown, West Virginia, United States of America

[3] Blanchette Rockefeller Neurosciences Institute, West Virginia University School of Medicine, Morgantown, West Virginia, United States of America

Correspondence:
Valeriya Gritsenko
vgritsenko@hsc.wvu.edu

Abstract

Human reaching movements require complex muscle activations to produce the forces necessary to move the limb in a controlled manner. How the complex kinetic properties of the limb and gravity contribute to the generation of the muscle activation pattern by the central nervous system (CNS) is a long-standing question in neuroscience. One common theory is that the CNS reduces the redundancies and complexities of the musculoskeletal system using motor primitives. These primitives are often obtained using decomposition methods based on shared variance across multiple signals. A critique of this technique is that the dependencies that exist due to the causal relationship between muscle activations and the resulting movement are difficult to disambiguate from neural primitives inherent in control signals. In the present study addressed this critique by examining the relationships between motor primitives extracted from muscle activity, muscle torques, and other motion signals. We hypothesized that the primitives obtained from muscle activity are more similar to kinetic primitives obtained from joint torques, than kinematic primitives obtained from joint angles and angular velocity signals. Eight healthy subjects pointed in virtual reality to visual targets arranged to create a standard center-out reaching task in three dimensions. Muscle activity and motion capture data were synchronously collected during the movements. Non-negative matrix factorization was then applied to muscle activity, muscle torques, and other motion signals (joint angles, angular velocities, gravitational torques, and other inertial torques) separately to reduce the dimensionality of data. Results show that the activation profiles of all NMF components were organized sequentially and correlated highly. The scaling of NMF components obtained from EMG and kinetic and kinematic signals correlated across multiple signal types. We found closer correspondence between NMF components obtained from EMG and gravitational torques, than those obtained from other torque signals or kinematic signals. Altogether, these results reject our hypothesis, suggesting that motor primitives do not consist of signals of a single modality. Our results also identify the kinetic signals for gravity compensation as the potential contributor to neural motor primitives that may be responsible for controlled transitions between arm postures during movement.

1. Introduction

The musculoskeletal anatomy of the body constitutes a complex dynamical system that is a challenge to control for the central nervous system (CNS). Some of the complexity is due to muscle redundancy that allows humans to perform complex tasks. Additional complexity is due to the forces associated with the inertia of the multi-joint limb, termed limb dynamics, which must also be accounted for by the CNS. Limb dynamics is commonly investigated through joint torques, or rotational forces, that arise during motion of the limb (Sainburg et al., 1995; 1999; Shabbott and Sainburg, 2008). This motion, commonly expressed as angular kinematics (position and velocity), can be used to derive joint torques for each independent direction of motion termed degree of freedom (DOF) using equations of motion. The goal is to derive the active torques that are generated because of muscle contractions in the presence of passive forces, such as those due to gravity or the interaction between connected segments (Dounskaia and Wang, 2014; Gentili et al., 2007; Le Seac'h and McIntyre, 2007; Papaxanthis et al., 2005). The latter passive interaction torques comprise a sizable amount of the overall

torques experienced during arm movement (Hollerbach and Flash, 1982). The compensation for interaction torques appears to be an important factor for the neural control of goal-directed movement (Debicki and Gribble, 2005; Gribble and Ostry, 1999; Gritsenko et al., 2009; 2011; Pigeon et al., 2003). Other passive torques arise due to gravity; these gravitational torques depend on the orientation of limb segments in space (Bastian et al., 1996). The compensation for gravitational torques is also important for motor control, as evidenced by altered patterns of movement errors and muscle activity of people moving in micro-gravity environments (Fisk et al., 1993; Papaxanthis et al., 1998; 2005; Pozzo et al., 1998). Altogether, the action of the CNS to control these passive torques can be observed at least partially through analysis of active muscle torques, which are the summed result of muscle contraction. Thus, muscle torques are a window into the interaction between the CNS and the musculoskeletal anatomy of the limb.

A prevalent explanation of how the CNS resolves the complexity of limb motor control is based on the idea of motor primitives, i.e. groups of muscles sharing the same common source of neural activation (Mussa Ivaldi, 1999; Mussa Ivaldi and Bizzi, 2000). These are usually extracted using decomposition methods, such as principle component analysis (PCA), or non-negative matrix factorization (NMF) (Ting, 2007; Tresch et al., 2006). These motor primitives have been shown to be most active for movements and in response to perturbations in specific directions, i.e. directionally tuned (d'Avella et al., 2006; Torres-Oviedo and Ting, 2007). They can also be scaled in both time and amplitude to adjust for changing speeds and distances during movement (d'Avella et al., 2008). It has also been suggested that motor primitives may be structured in such a way as to compensate for task-specific limb dynamics (Chvatal et al., 2011). Central to this concept is the idea that motor primitives can reduce the complexity of neural control signals by enabling the production of any movement from a smaller selection of control actions (Bizzi et al., 1991; Giszter et al., 1993) for a review see (d'Avella and Lacquaniti, 2013). However, the method of obtaining motor primitives using decomposition analyses has recently come under increased scrutiny due to the indivisible interaction and mutual dependencies between the neural control of muscular activations and the biomechanics of the resulting movement (Santello et al., 2013; Tresch and Jarc, 2009). For example, multiple independent DOFs of hand joints are known to be mechanically coupled through tendons that span several joints of a finger and the wrist. This reduces the overall range of possible motions to a much smaller subset of kinematic primitives, which could contribute to the motor primitives identified in muscle activations using decomposition methods (Valero-Cuevas et al., 2015). Furthermore, primitives obtained from joint kinematics and muscle activations were found to be mutually dependent (Kutch and Valero-Cuevas, 2012; Tagliabue et al., 2015). The latter study also shows that kinematic constraints can create the appearance of muscle primitives in simulated data, in which no neural primitives are expected a-priori.

In the current study, we further examine the transformation from muscle activation to movement to establish the role that motion kinematics and limb dynamics play in the generation of neural motor commands to muscles. The rationale for our approach is based on the examination of shared variance with NMF decomposition method across different types of motion-related signals. Among kinematic and kinetic signals, muscle activations are most closely related to kinetic signals such as active muscle torques described above. The muscle torques can in turn be split into two

components, 1) gravitational torques that only arise in the presence of gravity and 2) other inertial torques, including interaction torques, that are responsible for inter-joint coordination. Each of these components can be calculated for each joint DOF. However, across multiple joint DOFs, signals for each of these components are coupled through the kinematic chain of the limb. This coupling can be quantified using NMF to obtain kinetic primitives, which can then be compared to the primitives obtained from muscle activations. We hypothesize that primitives obtained from muscle activations are more similar to kinetic primitives obtained from torque components, than kinematic primitives obtained from joint angles and angular velocity signals. Support for this hypothesis would suggest that kinetic signals for gravity compensation and inter-joint coordination may comprise neural motor primitives.

2. Material and Methods

Eight healthy individuals (5 males, 3 females) with an average age of 24.8 ± 0.71 years old were recruited to perform a reaching "center-out" task. This study was carried out in accordance with the recommendations the Institutional Review Board of West Virginia University with written informed consent from all subjects. All subjects gave written informed consent in accordance with the Declaration of Helsinki. The protocol was approved by the Institutional Review Board of West Virginia University (Protocol # 1311129283). All subjects were right-hand dominant and reported no movement disorders and no major injuries to their right arm. Height, weight, and arm segment lengths were measured for each subject and used to adjust model parameters to create subject-specific dynamic models (see below).

Movements were instrumented using a virtual reality software (Vizard by Wolrdviz) and head set (Oculus Rift), which displayed 14 targets arranged in two perpendicular planes: the horizontal transverse plane and the vertical coronal plane (Fig. 1A). To reduce inter-subject variability in kinematic data, the target locations were adjusted for each subject based on the lengths of their arm segments, which ensured the same initial and final joint angles across all movement directions. The center target was placed so that initial arm posture was at 0-degree shoulder flexion, 90-degree elbow flexion, and a 0-degree wrist flexion. The distance from the center target to the peripheral targets was scaled to 30 percent of each subject's total arm length (from anterior acromial point to the distal end of the index finger). Each movement began with the subject starting at the center target and then moving to another visible target cued by target color change. Subjects were instructed to keep their wrist pronated and straight and move as quickly and accurately as possible. Movements to each target location were repeated 15 times and performed in a randomized order.

Fig. 1 near here

Arm and trunk movements were recorded with an active motion capture system (PhaseSpace, Impulse) at 480 frames per second. The light emitting diodes of the motion capture system were placed on anatomical landmarks according to best practice guidelines (Robertson et al., 2004). Electromyography (EMG) was recorded from twelve arm muscles at a rate of 2000 Hz (MA400-28 MotionLab Systems). Muscles recorded during the experiment included the pectoralis major (Pec), teres major (TrM), anterior deltoid (AD), posterior deltoid (PD), long and short heads of the biceps (BiL and BiS

respectively), lateral and long heads of the triceps (TrLa and TrLo respectively), brachioradialis (Br), flexor carpi ulnaris (FCU), flexor carpi radialis (FCR), and extensor carpi radialis (ECR). Motion capture and electromyography were synchronized using a custom circuit and triggering mechanism (Talkington et al., 2015). Motion capture and EMG data were imported into Matlab and processed as follows using custom scripts.

EMG data were high pass filtered at 40 Hz, bandpass filtered between 59 and 61 Hz to remove electrical background noise, rectified, and low pass filtered at 20 Hz. Motion capture data were low pass filtered at 10 Hz and interpolated with a cubic-spline. The maximum interpolated gap was 0.2 seconds. The onset and offset of movement was found based on the velocity of three hand LEDs changing by five percent of the maximum velocity for a given movement. Arm kinematics were obtained from motion capture by calculating Euler angles and angular velocity for five joint DOFs including shoulder (flexion/extension, abduction/adduction, pronation/supination), elbow (flexion/extension), and wrist (flexion/extension).

2.1.Limb dynamics

To calculate joint torques, an inverse dynamic model of the subject's arm was constructed in Simulink (MathWorks). The model comprised 5 DOFs as described above and three segments approximating inertial properties of the arm, forearm, and hand. Inertia of the segments was approximated with a cylinder of the length equal to that of the corresponding segment and a 3-cm radius. The masses and centers of mass for each segment were determined by their anthropometric ratios to the subjects' segment lengths and weight (Winter, 2009).

Angular kinematics averaged per movement direction and per subject was used in the subject-specific inverse model to calculate joint torques (Fig. 1B). These computed torques are proportional to the sum of all moments generated by muscles spanning the joints, so these torques are referred to as muscle torques in the rest of the manuscript. The numerical quality of inverse dynamic simulations was checked by running the same model in forward dynamics mode using the calculated torques as inputs and simulated angular kinematics as outputs. The simulated and experimental joint kinematics was compared, and the mean ± standard deviation of the root-mean-squared differences between them was 0.05 ± 0.02 radians across all DOFs.

To test the main hypothesis, the muscle torques obtained using the inverse model were separated into two components. To estimate the component of muscle torques responsible for inter-joint coordination without gravity, the inverse model was run without simulating external gravitational force. This resulted in muscle torques that would produce the same motion without gravity as that recorded in presence of gravity. Example of such torques would be the sum of muscle moments produced during motion in microgravity environment. Then the component of muscle torque that is needed to compensate for gravity was estimated as the difference between muscle torques with and without gravity as follows:

(1)

where τ_G is a vector of torques that only arise in the presence of gravity; τ_M is a vector of muscle torques around each DOF during simulations with gravity; τ_{MG0} is a

vector of computed torques around each DOF during simulations without gravity. If we assume that the torques produced without gravity are equal to the component of the motor command that is responsible for inter-joint coordination only, without gravity, then formula (1) can be rearranged as follows:

$$\tau_{MN} = \tau_M - \tau_{MG} \text{ , or}$$
$$\tau_M = \tau_{MN} + \tau_{MG} \quad (2)$$

where τ_{MN} is the component of muscle torque responsible for inter-joint coordination, i.e. interaction torques and other inertial torques excluding gravity, and τ_{MG} is the component of muscle torque responsible for the compensation for all torques due to gravity. Below, the former is referred to as MN torque, while the latter is referred to MG torque for simplicity.

2.2.Motor Primitive Decomposition

Motor primitives were extracted for each subject from EMG, kinematic and dynamic data separately using NMF (Berniker et al., 2009; Torres-Oviedo et al., 2006). To extract EMG primitives (NMF1 in Fig. 1B), rectified EMG signals were normalized to movement duration, averaged per movement direction, and low pass filtered at 10 Hz. To ensure muscle activations were unitless, maximum contraction values were calculated for each muscle across all movement directions and used to divide mean EMG for each movement direction. The resulting data matrix was comprised of 336 columns (12 EMG signals for 14 movements toward each virtual target and 14 return movements). Using the NMF algorithm described in Tresch et al. (Tresch et al., 1999), EMG primitives were extracted for each subject.

$$m(t) = \sum_{i=1}^{N} C_i \; W_i(t) \quad (3)$$

where $m(t)$ is the EMG matrix of average activity of all muscles during all movements at time t ; N is the number of primitives; C_i is the array of weights for primitive i for each muscle and movement; and $W_i(t)$ is the activation of primitive i at time t (Fig. 2). The number of EMG primitives was increased until the variance accounted for (VAF) in EMG reached 95%.

Fig. 2 near here

To extract muscle-torque primitives, a data matrix was constructed for each subject that included muscle torques for each DOF and each movement direction (NMF2 in Fig. 1B). The signals were rectified then normalized to the largest value of the signal for each DOF across all movement directions. The resulting data matrix was comprised of 120 columns (5 muscle torque signals for the 28 movement directions). NMF was applied to this data with the same criteria described above.

$$\tau_M(t) = \sum_{i=1}^{N} A_i \; Y_i(t) \quad (4)$$

where $\tau_M(t)$ is the muscle torque matrix for all signals per DOF per movement

direction; N is the number of primitives; A_i is the weight matrix for primitive i for each DOF and movement; and $Y_i(t)$ is the activation profile of the corresponding primitive i.

To extract mechanical primitives, a data matrix was constructed that included joint angles, angular velocity, MG torque and MN torque for each DOF (NMF3 in Fig. 1B). The signals were averaged across the fifteen repetitions of each movement direction. The same rectification, and normalization procedures were applied to the signals as described above for muscle torques. This ensured the same scale and unit independence across all signals. The data matrix comprised 560 columns (20 kinematic and kinetic signals for the 28 movement directions). NMF was applied to this data with the same criteria described above.

$$d(t) = \sum_{i=1}^{N} B_i \; X_i(t) \qquad (5)$$

where $d(t)$ is the matrix of average profiles for all signals; N is the number of primitives; B_i is the weight matrix for primitive i for each signal; and $X_i(t)$ is the activation profile of the corresponding primitive i.

The rectification procedure changed the profiles of the muscle and inertial torques, which could affect the comparison between motor primitives based on these signals and EMG. Rectification of inertial torques poses less of a problem, because these signals contain two readily identifiable phases of acceleration and deceleration that match the actions of individual muscles. Rectification of these signals results in profiles with two burst-like shapes that correspond to the timing of the two phases. However, rectification of muscle torques results in more variable changes in their profiles that are not easily linked to specific movement phases. To address this concern, we tested the validity of NMF on the rectified torque signals to accurately capture the relationship between signals. For this we substituted equations (4) and (5) into equation (2). Given that our analysis, described below, found highly correlated NMF temporal profiles across signals (Fig. 4), the resulting equation can be reduced as follows:

$$A_i = B_{i1} + B_{i2} \qquad (6)$$

where for primitive i, NMF weight A for each muscle torque signal is the sum of NMF weights B_1 and B_2 for MN and MG torques respectively for corresponding DOFs. The NMF weights calculated from rectified muscle torques differed from those calculated using equation (6) between 1 ± 4 % and 3 ± 6 % across subjects. The threshold for VAF was 95%, which puts the differences in weights between the two methods below this threshold. This shows that NMF on rectified muscle torque signals captures accurately the linear relationships between those and other signals.

Resulting activations $W_i(t)$, $X_i(t)$, and, $Y_i(t)$ were normalized from zero to one for each subject. Normalization values were obtained by calculating the peak value from each subject's activation. For comparisons across signal types and across subjects, activations $W_i(t)$, $X_i(t)$, and, $Y_i(t)$ were sorted per the relative timing of their maximal peak and assigned a letter in alphabetical order (Fig. 2A).

To maintain the relative relationship between the weights and activations, NMF weights, C_i, A_i, and B_i were multiplied by the normalization value of the corresponding activation. This ensured that the variance for each movement direction was now captured

by the NMF weights, not activations. Thus, NMF weights were then used to compare directional tuning between EMG, muscle-torque, and mechanical primitives. Coefficient of determination (r^2) was used as measures of similarity between the NMF weights obtained from different signals, NMF1, NMF2, and NMF3. Note that signals used for all NMF analyses were unitless. Correlation matrices were calculated between NMF weights C_i and A_i, and between NMF weights C_i and B_i across corresponding directions of movement for first and last primitive only.

2.3.Statistical analysis

The statistical analysis of r^2 values was done using repeated measures analysis of variance (rANOVA) in MATLAB. Separate rANOVA tests were applied to r^2 values calculated between EMG and muscle-torque primitives (rANOVA1: weights from NMF1 vs. NMF2) and between EMG and mechanical primitives (rANOVA2: weights from NMF1 vs. NMF3). rANOVA1 included 2 factors, Joint and Primitive factor. The Joint factor grouped r^2 values based on the joint the signals spanned, comprising 3 levels for shoulder, elbow, and wrist. The Primitive factor grouped r^2 values based on the timing of the activation profile of each primitive, comprising 2 levels for the first primitive A and the last primitive C or E (Fig. 4). rANOVA2 included 3 factors, Joint and Primitive factors as in rANOVA1 and a Signal factor. The Signal factor grouped r^2 values based on the types of signals used in NMF3, comprising 4 levels for joint angles, angular velocity, MG torque, and MN torque. Post-hoc multiple comparisons were used to further examine significant interactions.

Cross-correlation analysis was used to compare activations $W_i(t)$, $X_i(t)$, and, $Y_i(t)$. The temporal shifts that produced the highest correlations between each pair of activations were converted into the time domain from the normalized number of samples by using the mean duration of movement per subject. Positive lag times indicate that the second signal follows the first in each pair. A negative lag time indicates that the second signal precedes the first.

The relationships between peaks of activation for subsequent primitives obtained with NMF1, and between peaks of activation for corresponding primitives obtained with NMF1 vs. NMF2 and NMF3 were quantified using a linear regression. The same peaks of each activation used for the classification of the primitives (Fig. 2A) were used in this regression analysis.

3. Results

The angular kinematics of pointing to targets in virtual reality was highly consistent, as demonstrated by the low standard deviations of angular kinematics across the fifteen repetitions of each movement (Fig. 3A). The peak velocity of these movements ranged from 1.2 to 3.3 meters per second, which illustrates subjects' preferred speeds in response to instructions to point as quickly and accurately as possible (Fig. 3B). The consistent kinematics are attributed to the very consistent muscle torques, whose temporal profiles varied little across subjects (Fig. 3C). However, muscle activity was highly consistent within subjects (Fig. 3F), but varied between subjects.

Fig. 3 near here.

Muscle torques were divided into gravitational and other inertial torques (termed MG and MN torques) as described above. Gravitational torques were consistent within and across subjects and showed similar temporal profiles to joint angles (Fig. 3D). Inertial torques were also consistent within and across subjects. MN torques had activation profiles that were distinct from MG torque profiles (Fig. 3E) and similar to acceleration profiles derived from angular kinematics. In a given movement, MG torques tended to vary in a single direction increasing or decreasing in amplitude, while the MN torques usually comprised acceleration and deceleration phases characteristic of a bell-shaped velocity profile. For multiple movements, torques of the same type were coupled across DOFs (Figs 3D and 3E).

NMF1 on EMGs showed that between 2 and 5 EMG primitives were necessary to reach a VAF = 96.6 $^{\pm}$ 0.9 %. The primitives were labeled A through E, corresponding to the order in which the peak of the activation profile occurred. The activation profile of primitive A peaked at 1.0 ± 2.1 % of the average movement duration, followed by primitive B at 16.7 ± 14.0 %, primitive C at 18.5 ± 19.8 %, primitive D at 28.6 ± 13.6 %, and primitive E at 89.0 ± 11.0 % (Fig. 4, red lines).

Fig. 4 near here

NMF2 on muscle torques showed that, unlike NMF1, only 3 muscle-torque primitives were required to reach a VAF = 96.4 ± 0.0 % across subjects. Primitives were labeled as A through C based on their temporal sequence as described above. Activation profiles of primitive A peaked at 2.1 ± 4.5 % of the average movement duration, followed by primitive B at 35.7 ± 15.7 %, and primitive C at 99.7 ± 1.0 % (Fig. 4, blue lines).

NMF3 on mechanical signals showed that 3 mechanical primitives were required to reach a VAF = 96.8 ± 0.3% across subjects, same as the number derived by NMF2. Mechanical primitives were labeled as described above; the activation of primitive A peaked at 0.3 ± 0.0 % of the average movement duration, followed by primitive B at 42.2 ± 17.3 %, and primitive C at 98.5 ± 3.3 % (Fig. 4, black lines).

The activation profiles obtained with NFM represent the amount of recruitment of a given primitive and may be more closely related to the temporal evolution of neural commands. The activation profiles were very similar not only across subjects, but also across signal types. The activation of sequential EMG primitives was highly correlated with peak correlation coefficients across subjects ranging from 0.84 ± 0.07 between the first and second EMG primitive to 0.56 ± 0.11 between the first and last EMG primitive. These peak correlations occurred at lag times that were increasing on average at 170 ms intervals (Fig. 5A). The activation profiles of EMG primitives peaked at times that were linearly increasing (r^2 = 0.94; Fig. 5B). Furthermore, the activations of overlapping EMG and muscle-torque primitives were highly correlated with peak correlation coefficients across subjects ranging from 0.94 ± 0.03 between the first EMG and first muscle-torque primitive to 0.53 ± 0.05 between the first EMG and last muscle-torque primitive. These peak correlations occurred at incremental lag times (Fig. 5C). The activation profiles of EMG primitives peaked at times that were linearly related to the peaks in the corresponding activations of muscle-torque primitives (r^2 = 0.97; Fig. 5D). Similar relationships were observed between the activations of EMG and mechanical primitives (Figs 5E and 5F; r^2 = 0.96). This shows that the activation profiles of all primitives were

organized sequentially and correlated highly.

Fig. 5 near here

3.1.The overlap in directional tuning between different types of primitives

To determine if EMG primitives have the same directional tuning as muscle-torque primitives, shared variance (r^2) between weights from NMF1 and NMF2 across all movement directions was calculated for the first and last primitive for each subject. Separate comparison for each primitive ensured that the temporal distribution of the primitives obtained from EMG and muscle-torques were matched (Fig. 4). The r^2 values between NMF weights were small for most signal combinations, which indicates little overlap between directional tunings of EMG primitives and muscle-torque primitives (Fig. 6). There were some differences in r^2 values of both primitives for signals originating from the different joints, but post-hoc comparisons revealed no consistent effects (Table 1).

Fig. 6 and Table 2 near here

To determine if EMG primitives have the same directional tuning as mechanical primitives, shared variance (r^2) between weights from NMF1 and NMF3 across all movement directions was calculated for the first and last primitive for each subject. Separate comparison for each primitive ensured that the temporal distribution of the primitives obtained from EMG and kinematic and kinetic signals are matched (Fig. 4). The r^2 values between NMF weights were larger than in previous analysis for many signal combinations (Fig. 7). In the beginning of movement, the mean r^2 for MG and MN torque signals was larger than the mean r^2 for velocity and angle signals for corresponding DOFs in 9 (out of 12) muscles, while the opposite was true for 1 muscle (TrLa) and no change was observed in 2 muscles (BiS and TrLo; Fig. 7, Primitive A). At the end of movement, the mean r^2 for MG and MN torque signals was larger than the mean r^2 for velocity and angle signals for corresponding DOFs in only 5 muscles (FCU, BiL, BiS, TriLA, and AD), while the opposite was true in 5 other muscles (FCR, ECR, Br, TrLo, and Pec) and no change was observed in 2 muscles (TrM and PD; Fig. 7, Primitive C/E). Larger r^2 values were observed between NMF weights from EMG signals and MG torques compared to those from EMG signals and MN torques and from EMG signals and joint velocity, but only for the last primitive (Fig. 7A, Table 2).

Fig. 7 and Table 2 near here

Some of the observed differences between the directional tuning of muscle-torque, mechanical, and EMG primitives may be due to the different number of primitives obtained from noisier EMG signals. To address this issue, we have compared NMF weights from subjects with the number of EMG primitives matching the number of muscle-torque and mechanical primitives, to the NMF weights from the rest of the subjects with unmatched number of EMG primitives. The mean difference ± confidence interval between the NMF weights from 3 subjects with three EMG primitives and 5 subjects with other numbers of EMG primitives (2, 4, and 5) was -0.005 ± 0.025, which

was not significant ($p = 0.65$). This shows that the difference between muscle-torque, mechanical, and EMG primitives is not due to the larger noise in EMG signals.

4. Discussion

The hypothesis of our study was that primitives obtained from muscle contractions are more similar to kinetic primitives obtained from joint torques, than kinematic primitives obtained from joint angles and angular velocity signals. We found that when controlling for temporal evolution of primitives, the spatial distribution of EMG and MG primitives overlapped more than that of EMG and joint velocity primitives. However, no other statistical differences between the spatial distributions of kinetic and kinematic signals were observed. These results led us to reject the main hypothesis. Instead, our results suggest that motor primitives do not consist of signals of a single modality, but rather combine both kinetic and kinematic signals.

The transformation from muscle activation to motion is non-linear and includes second order differential dynamics. Here, we have defined motor primitives as functional components of joint torques that are related to either gravity or inter-joint coordination. Deriving primitives from dynamical signals like joint torques should result in a more linear relationship with neural control signals, if those primitives capture accurately the dynamics of neural signals. Indeed, we have found more shared variance between mechanical primitives and EMG primitives than between muscle-torque and EMG primitives. In particular, the primitive at the end of movement derived from the gravity torque component shared the most variance with the corresponding EMG primitive. In contrast, the primitive derived from joint velocity shared the least variance with the corresponding EMG primitive. This provides further supporting evidence for the dynamical, rather than kinematic, nature of neural motor commands (Caminiti et al., 1990; 1991; Scott, 1997; Scott and Kalaska, 1997). Neural commands may comprise both phasic and tonic components, similar to those identified in EMG during 3D pointing movements (d'Avella et al., 2008; Flanders, 1991). The required scaling of a hypothetical tonic command for different movement directions could reflect the corresponding changes in gravitational load on the arm, i.e. as predicted by the MG torque components in our study. Thus, the hypothetical tonic command compensating for gravity may constitute an anticipatory postural adjustment that accompanies movement (Massion, 1992). Alternatively, the hypothetical tonic command may be a spinal feedback response to changing gravitational load signaled by proprioceptors. Our results support the latter by indicating more robust differences in the shared variance at the end of movement (Fig. 7 and Table 2). The mechanism responsible for a feedback compensation for gravity may be akin to positive force feedback during locomotion based on afferent feedback from Golgi tendon organs to maintain load bearing (Pearson and Collins, 1993; Prochazka et al., 1997).

Deriving motor primitives with decomposition methods is confounded by the indivisible interactions between muscle activations and the resulting movement (Santello et al., 2013; Tresch and Jarc, 2009). In other words, it is difficult to determine whether correlations between muscle activations cause correlations between motion-related signals, or it is the other way around. We too have observed the high degree of shared variance within all motion-related signals as evidenced by only three primitives present in both the kinematic and dynamic signals, consistent with results reported previously for reaching movements (Chiovetto et al., 2013). However, we have also shown that NMF

weights, while being directionally tuned as reported previously (Chiovetto et al., 2010; 2013; d'Avella et al., 2006; Torres-Oviedo and Ting, 2007), were tuned very differently when obtained from kinematic, or kinetic, or EMG signals (Fig. 3). We observed a rather small subset of pairs of signals with more than 10% shared variance, many of which did not come from the same joint (Fig. 7). This suggests that the method of examining the overlap in directional tuning while controlling for common temporal dynamics may offer a way to identify the modality of control signals and to disambiguate it from inherent relationships across multiple types of motion-related signals.

The CNS is a hierarchal dynamical system with recurrent feedback loops (Prochazka and Yakovenko, 2007; Shenoy et al., 2013). The output of this system has been observed in electrophysiological studies in animals as sequential neural primitives that are recruited during a reaching motion and correspond to the different phases of movement (Yakovenko et al., 2011). Similarly, we have observed highly correlated activations of sequential EMG primitives (Fig. 4). These activations were shifted in time at physiological delays (Fig. 5), which are consistent with transcortical feedback loops (Lee et al., 1983). These results suggest that the timing of the activations of the NMF primitives may indicate the timing of feedback processing within the motor system. The predictable sequence of peaks in the activation of primitives may be a useful tool for diagnosing neural dysfunction (Olesh and Gritsenko, 2017).

Our results are also consistent with the idea that there are no “true” muscle primitives. This argument is illustrated by a recent study, which found that muscles are recruited flexibly without a consistent pattern of groupings across movements (Kutch et al., 2008). In our results these flexible muscle groupings may appear as highly variable NMF weights, which vary in directional tuning between movement planes and forward and backward directions. Such flexible recruitment may be enabled by the dynamical nature of the nervous system, which could fully imbed the complex limb dynamics and its interaction with the external world in dedicated neural modules called internal models (Gomi and Kawato, 1997; Lackner and Dizio, 1994; Sabes, 2000; Shadmehr and Mussa Ivaldi, 1994; Wolpert and Kawato, 1998). These internal models or embodied neural dynamical systems would calculate the required muscle activation patterns specifically for a given class of similar movements, which may represent a learned task or a unit of motor memory (Haruno et al., 2001; Wolpert and Kawato, 1998).

4.1.Conclusions

In conclusion, our results have shown that when controlling for the temporal evolution of primitives, the primitives obtained from muscle activity and gravitational torques shared the most variance. This suggests that motor primitives do not consist of signals of a single modality, but rather combine both kinetic and kinematic signals.

Conflict of Interest Statement

The authors declare no conflicts of interest.

Authors and Contributors

EO contributed to the design of the study, subject recruitment, data collection, data analysis, and writing of the manuscript. BP contributed to the data collection and analysis, and to writing of the manuscript. VG contributed to the design of the study,

analysis of data, and writing of the manuscript.

Funding

This research was sponsored by NIH/NIGMS U54GM104942 (EO) providing student fellowship, NIH P20GM109098 providing salary support (VG, BP) and supplies, NIH P30GM103503 providing equipment support. The content is solely the responsibility of the authors and does not necessarily represent the official views of the NIH.

Acknowledgments

The authors wish to thank Dr. Sergiy Yakovenko for his contribution to the discussion of analysis in this study and Dr. Robert L. Goodman and Dr. Amy J. Bastian for their critical review of this manuscript.

References

Bastian, A. J., Martin, T. A., Keating, J. G., and Thach, W. T. (1996). Cerebellar ataxia: abnormal control of interaction torques across multiple joints. *J Neurophysiol* 76, 492–509.

Berniker, M., Jarc, A., Bizzi, E., and Tresch, M. C. (2009). Simplified and effective motor control based on muscle synergies to exploit musculoskeletal dynamics. *PNAS* 106, 7601–7606. doi:10.1073/pnas.0901512106.

Bizzi, E., Mussa Ivaldi, F., and Giszter, S. (1991). Computations underlying the execution of movement: a biological perspective. *Science* 253, 287–291.

Caminiti, R., Johnson, P. B., and Urbano, A. (1990). Making arm movements within different parts of space: dynamic aspects in the primate motor cortex. *J Neurosci* 10, 2039–2058.

Caminiti, R., Johnson, P., Galli, C., Ferraina, S., and Burnod, Y. (1991). Making arm movements within different parts of space: the premotor and motor cortical representation of a coordinate system for reaching to visual targets. *J Neurosci* 11, 1182–1197.

Chiovetto, E., Berret, B., and Pozzo, T. (2010). Tri-dimensional and triphasic muscle organization of whole-body pointing movements. *Neurosci* 170, 1223–1238. doi:10.1016/j.neuroscience.2010.07.006.

Chiovetto, E., Berret, B., Delis, I., Panzeri, S., and Pozzo, T. (2013). Investigating reduction of dimensionality during single-joint elbow movements: a case study on muscle synergies. *Front Comput Neurosci* 7, 1:12. doi:10.3389/fncom.2013.00011.

Chvatal, S. A., Torres-Oviedo, G., Safavynia, S. A., and Ting, L. H. (2011). Common muscle synergies for control of center of mass and force in nonstepping and stepping postural behaviors. *J Neurophysiol* 106, 999–1015. doi:10.1152/jn.00549.2010.

d'Avella, A., and Lacquaniti, F. (2013). Control of reaching movements by muscle synergy combinations. *Front Comput Neurosci* 7, 42. doi:10.3389/fncom.2013.00042.

d'Avella, A., Fernandez, L., Portone, A., and Lacquaniti, F. (2008). Modulation of phasic and tonic muscle synergies with reaching direction and speed. *J Neurophysiol* 100, 1433–1454. doi:10.1152/jn.01377.2007.

d'Avella, A., Portone, A., Fernandez, L., and Lacquaniti, F. (2006). Control of fast-reaching movements by muscle synergy combinations. *Journal of Neuroscience* 26, 7791–7810. doi:10.1523/JNEUROSCI.0830-06.2006.

Debicki, D. B., and Gribble, P. L. (2005). Persistence of inter-joint coupling during single-joint elbow flexions after shoulder fixation. *Experimental brain research* 163, 252–257.

Dounskaia, N. V., and Wang, W. (2014). A preferred pattern of joint coordination during arm movements with redundant degrees of freedom. *J Neurophysiol* 112, 1040–1053. doi:10.1152/jn.00082.2014.

Fisk, J., Lackner, J. R., and Dizio, P. (1993). Gravitoinertial force level influences arm movement control. *J Neurophysiol* 69, 504–511.

Flanders, M. (1991). Temporal patterns of muscle activation for arm movements in three-dimensional space. *J Neurosci* 11, 2680–2693.

Gentili, R., Cahouet, V., and Papaxanthis, C. (2007). Motor planning of arm movements is direction-dependent in the gravity field. *Neurosci* 145, 20–32. doi:10.1016/j.neuroscience.2006.11.035.

Giszter, S. F., Mussa-Ivaldi, F. A., and Bizzi, E. (1993). Convergent force fields organized in the frog's spinal cord. *J Neurosci* 13, 467–491.

Gomi, H., and Kawato, M. (1997). Human arm stiffness and equilibrium-point trajectory during multi-joint movement. *Biol Cybern* 76, 163–171.

Gribble, P. L., and Ostry, D. J. (1999). Compensation for Interaction Torques During Single- and Multijoint Limb Movement. *J Neurophysiol* 82, 2310–2326.

Gritsenko, V., Kalaska, J. F., and Cisek, P. (2011). Descending corticospinal control of intersegmental dynamics. *J Neurosci* 31, 11968–11979. doi:10.1523/JNEUROSCI.0132-11.2011.

Gritsenko, V., Yakovenko, S., and Kalaska, J. F. (2009). Integration of predictive feedforward and sensory feedback signals for online control of visually guided movement. *J Neurophysiol* 102, 914–930. doi:10.1152/jn.91324.2008.

Haruno, M., Wolpert, D. M., and Kawato, M. (2001). Mosaic model for sensorimotor

learning and control. *Neural Comput* 13, 2201–2220. doi:10.1162/089976601750541778.

Hollerbach, J. M., and Flash, T. (1982). Dynamic interactions between limb segments during planar arm movement. *Biol Cybern* 44, 67–77.

Kutch, J. J., and Valero-Cuevas, F. J. (2012). Challenges and new approaches to proving the existence of muscle synergies of neural origin. *PLoS Comput. Biol.* 8, e1002434. doi:10.1371/journal.pcbi.1002434.

Kutch, J. J., Kuo, A. D., Bloch, A. M., and Rymer, W. Z. (2008). Endpoint force fluctuations reveal flexible rather than synergistic patterns of muscle cooperation. *J Neurophysiol* 100, 2455–2471. doi:10.1152/jn.90274.2008.

Lackner, J. R., and Dizio, P. (1994). Rapid adaptation to Coriolis force perturbations of arm trajectory. *J Neurophysiol* 72, 299–313.

Le Seac'h, A. B., and McIntyre, J. (2007). Multimodal reference frame for the planning of vertical arms movements. *Neurosci Lett* 423, 211–215. doi:10.1016/j.neulet.2007.07.034.

Lee, R. G., Murphy, J. T., and Tatton, W. G. (1983). Long-latency myotatic reflexes in man: mechanisms, functional significance, and changes in patients with Parkinson's disease or hemiplegia. *Adv Neurol* 39, 489–508.

Massion, J. (1992). Movement, posture and equilibrium: interaction and coordination. *Prog Neurobiol* 38, 35–56.

Mussa Ivaldi, F. (1999). Modular features of motor control and learning. *Curr Opin Neurobiol* 9, 713–717.

Mussa Ivaldi, F., and Bizzi, E. (2000). Motor learning through the combination of primitives. *Philos Trans R Soc Lond B* 355, 1755–1769.

Olesh, E. V., and Gritsenko, V. (2017). Linking post-stroke movement impairment to mechanistic changes in the neural control of movement. In: *Combined Sections Meeting;* 2017 Feb 15-18; San Antonio, TX. p. 1280.

Papaxanthis, C., Pozzo, T., and McIntyre, J. (2005). Kinematic and dynamic processes for the control of pointing movements in humans revealed by short-term exposure to microgravity. *Neurosci* 135, 371–383. doi:10.1016/j.neuroscience.2005.06.063.

Papaxanthis, C., Pozzo, T., Popov, K. E., and McIntyre, J. (1998). Hand trajectories of vertical arm movements in one-G and zero-G environments. Evidence for a central representation of gravitational force. *Experimental brain research* 120, 496–502.

Pearson, K. G., and Collins, D. F. (1993). Reversal of the influence of group Ib afferents

from plantaris on activity in medial gastrocnemius muscle during locomotor activity. *J Neurophysiol* 70, 1009–1017.

Pigeon, P., Bortolami, S., Dizio, P., and Lackner, J. R. (2003). Coordinated turn-and-reach movements. I. Anticipatory compensation for self-generated Coriolis and interaction torques. *J Neurophysiol* 89, 276–289. doi:10.1152/jn.00159.2001.

Pozzo, T., Papaxanthis, C., Stapley, P., and Berthoz, A. (1998). The sensorimotor and cognitive integration of gravity. *Brain Res Brain Res Rev* 28, 92–101.

Prochazka, A., and Yakovenko, S. (2007). The neuromechanical tuning hypothesis. *Prog Brain Res* 165, 255–265. doi:10.1016/S0079-6123(06)65016-4.

Prochazka, A., Gillard, D. M., and Bennett, D. J. (1997). Positive force feedback control of muscles. *J Neurophysiol* 77, 3226–3236.

Sabes, P. N. (2000). The planning and control of reaching movements. *Curr Opin Neurobiol* 10, 740–746.

Sainburg, R. L., Ghez, C., and Kalakanis, D. (1999). Intersegmental Dynamics Are Controlled by Sequential Anticipatory, Error Correction, and Postural Mechanisms. *J Neurophysiol* 81, 1045–1056.

Sainburg, R. L., Ghilardi, M., Poizner, H., and Ghez, C. (1995). Control of limb dynamics in normal subjects and patients without proprioception. *J Neurophysiol* 73, 820–835.

Santello, M., Baud-Bovy, G., and Jörntell, H. (2013). Neural bases of hand synergies. *Front Comput Neurosci* 7, 23. doi:10.3389/fncom.2013.00023.

Scott, S. H. (1997). Comparison of onset time and magnitude of activity for proximal arm muscles and motor cortical cells before reaching movements. *J Neurophysiol* 77, 1016–1022.

Scott, S. H., and Kalaska, J. F. (1997). Reaching movements with similar hand paths but different arm orientations. I. Activity of individual cells in motor cortex. *J Neurophysiol* 77, 826–852.

Shabbott, B. A., and Sainburg, R. L. (2008). Differentiating between two models of motor lateralization. *J Neurophysiol* 100, 565–575. doi:10.1152/jn.90349.2008.

Shadmehr, R., and Mussa Ivaldi, F. (1994). Adaptive representation of dynamics during learning of a motor task. *J Neurosci* 14, 3208–3224.

Shenoy, K. V., Sahani, M., and Churchland, M. M. (2013). Cortical control of arm movements: a dynamical systems perspective. *Annu Rev Neurosci* 36, 337–359. doi:10.1146/annurev-neuro-062111-150509.

Tagliabue, M., Ciancio, A. L., Brochier, T., Eskiizmirliler, S., and Maier, M. A. (2015). Differences between kinematic synergies and muscle synergies during two-digit grasping. *Front Hum Neurosci* 9, 1–17. doi:10.3389/fnhum.2015.00165.

Talkington, W. J., Pollard, B. S., Olesh, E. V., and Gritsenko, V. (2015). Multifunctional Setup for Studying Human Motor Control Using Transcranial Magnetic Stimulation, Electromyography, Motion Capture, and Virtual Reality. *J Vis Exp*, e52906–e52906. doi:10.3791/52906.

Ting, L. H. (2007). Dimensional reduction in sensorimotor systems: a framework for understanding muscle coordination of posture. *Prog Brain Res* 165, 299–321. doi:10.1016/S0079-6123(06)65019-X.

Torres-Oviedo, G., and Ting, L. H. (2007). Muscle synergies characterizing human postural responses. *J Neurophysiol* 98, 2144–2156. doi:10.1152/jn.01360.2006.

Torres-Oviedo, G., Macpherson, J. M., and Ting, L. H. (2006). Muscle synergy organization is robust across a variety of postural perturbations. *J Neurophysiol* 96, 1530–1546. doi:10.1152/jn.00810.2005.

Tresch, M. C., and Jarc, A. (2009). The case for and against muscle synergies. *Curr Opin Neurobiol* 19, 601–607. doi:10.1016/j.conb.2009.09.002.

Tresch, M. C., Cheung, V. C. K., and d'Avella, A. (2006). Matrix factorization algorithms for the identification of muscle synergies: evaluation on simulated and experimental data sets. *J Neurophysiol* 95, 2199–2212. doi:10.1152/jn.00222.2005.

Tresch, M. C., Saltiel, P., and Bizzi, E. (1999). The construction of movement by the spinal cord. *Nat Neurosci* 2, 162–167. doi:10.1038/5721.

Valero-Cuevas, F. J., Cohn, B. A., Yngvason, H. F., and Lawrence, E. L. (2015). Exploring the high-dimensional structure of muscle redundancy via subject-specific and generic musculoskeletal models. *J Biomech* 48, 2887–2896. doi:10.1016/j.jbiomech.2015.04.026.

Winter, D. A. (2009). *Biomechanics and Motor Control of Human Movement*. 4 ed. Hoboken, New Jersey: John Wiley & Sons.

Wolpert, D. M., and Kawato, M. (1998). Multiple paired forward and inverse models for motor control. *Neural Netw* 11, 1317–1329.

Yakovenko, S., Krouchev, N. I., and Drew, T. (2011). Sequential activation of motor cortical neurons contributes to intralimb coordination during reaching in the cat by modulating muscle synergies. *J Neurophysiol* 105, 388–409. doi:10.1152/jn.00469.2010.

Figure and Table Legends

Figure 1. Experimental setup and analysis flow. (A) Illustration showing the locations of reaching targets, arranged in a semi-spherical pattern in VR, relative to the physical location of the subject. The central target is shown in red and one of the goal targets is shown in green. (B) Schematic representation of analysis flow. IDM stands for inverse dynamic model. NMF1, NMF2, and MNF3 indicate separate analyses applied to EMG, muscle torque, and other kinetic and kinematic data respectively. Mathematical symbols match those used in formulae in Methods.

Figure 2. Examples of NMF analysis of EMG. (A) Average muscle activation (solid lines) from two muscles during one movement for one subject (plotted with standard deviation from 15 repetitions of the same movement). The subject shown here required 4 primitives for EMG VAF > 95%. The activation profiles from these primitives were categorized as A, B, D and E based on the order of their peaks (see Methods). (B) Illustration of weights across movements for the two EMG signals. The NMF weights for each primitive and each movement direction is the distance in the polar coordinates, the angle is based on the direction of motion in one plane, or the reaching target location relative to the starting target.

Figure 3. Example motion signals, muscle activity, and corresponding NMF weights for a single subject. The central polar plots show normalized weights for the first NMF primitive plotted as in Fig. 2B. The temporal profiles of signals from which the NMF weights were obtained are shown around the polar plots in matching colors. All signals are normalized in time and amplitude as described in Methods for NMF analysis. (A) Joint angles in time and corresponding weights from NMF3. Averages (solid lines) and standard deviations (shaded areas) are across movement repetitions. (B) Angular velocity in time and corresponding weights from NMF3, formatted as in (A). (C) Muscle torques in time and corresponding weights from NMF2, formatted as in (A). (D) MG torque in time and corresponding weights from NMF3, formatted as in (A). (E) MN torque in time and corresponding weights from NMF3, formatted as in (A). (F) EMG signals in time and corresponding weights from NMF1. Averages (solid lines) and standard errors of the mean (shaded areas) are across movement repetitions. Muscle abbreviations are as described in Methods.

Figure 4. Temporal activation profiles of EMG, muscle-torque, and mechanical primitives. Average normalized activation profiles (solid lines) and standard deviations (shaded area) across all eight subjects are plotted for each activation. The activation profiles were arranged based on the occurrence of the first peak and labeled A through C for muscle-torque (blue) and mechanical (black) primitives. EMG activation profiles were labeled A through C (red). Titles show the labels for activation profiles from each type of primitive that are plotted on the same plot. Both temporal and amplitude values for all activation profiles were normalized as described in Methods.

Figure 5. Cross-correlation lag times and peaks of NMF activation profiles. (A) Lag times that correspond to maximal correlations between activation profiles of EMG primitives. Red lines indicate the median value across subjects with the 25th and 75th percentiles marked by the edges of each box. (B) Peak times of each activation profile of EMG primitive per subject. (C) Lag times that correspond to maximal correlations between activation profiles of EMG and muscle-torque primitives. Plot is formatted as in A. (D) Peak times of activation profiles of EMG primitives and the

corresponding muscle-torque primitives per subject. (E) Lag times that correspond to maximal correlations between activation profiles of EMG primitives and mechanical primitives. Plot is formatted as in A. (F) Peak times of activation profiles of EMG primitives and the corresponding mechanical primitives per subject.

Figure 6. Shared variance between weights from NMF1 on EMG and NMF2 on muscle torques. The colors of circles indicate r2 values between weights for corresponding signals across all movements averaged across subjects. Muscle abbreviations are as described in Methods. F/E stands for flexion/extension; Ab/Ad stands for abduction/adduction; Pro/Sup stands for pronation/supination.

Figure 7. Shared variance between weights from NMF1 on EMG and NMF3 on kinematic and kinetic signals. The colors of circles indicate r2 values between weights for corresponding signals across all movements averaged across subjects. Muscle abbreviations are as described in Methods. F/E stands for flexion/extension; Ab/Ad stands for abduction/adduction; Pro/Sup stands for pronation/supination.

Tables

Table 1. rANOVA1 on shared variance between weights of NMF 1 on EMG and weights of NMF2 on muscle torques.

rANOVA	**Degrees of Freedom**	***F***	***p***
Factors	119	3.58	**0.01**
Gender x Factors	119	0.84	0.53
Multiple comparisons		**Difference**	***p***
Factor Primitive	A - C/E	-0.02	*0.09*
Factor Joint	across - within	0.002	*0.65*

Table 2. rANOVA2 on shared variance between weights of NMF 1 on EMG and weights of NMF3 on kinematic and kinetic signals.

rANOVA	**Degrees of Freedom**	***F***	***p***
Factors	479	3.32	**0.02**
Gender x Factors	479	0.88	0.51
Multiple comparisons		**Difference**	***p***
Primitive A	velocity - angle	-0.023	0.15
Primitive A	velocity - MG torque	-0.003	0.93
Primitive A	velocity - MN torque	0.013	0.64

rANOVA	**Degrees of Freedom**	***F***	***p***
Primitive A	angle - MG torque	0.019	0.07
Primitive A	angle - MN torque	0.036	0.18
Primitive A	MG torque - MN torque	0.017	0.45
Primitive C/E	velocity - angle	-0.012	0.47
Primitive C/E	velocity - MG torque	-0.033	**0.01**
Primitive C/E	velocity - MN torque	0.024	0.1
Primitive C/E	angle - MG torque	-0.021	0.16
Primitive C/E	angle - MN torque	0.036	0.05
Primitive C/E	MG torque - MN torque	0.056	**0.02**

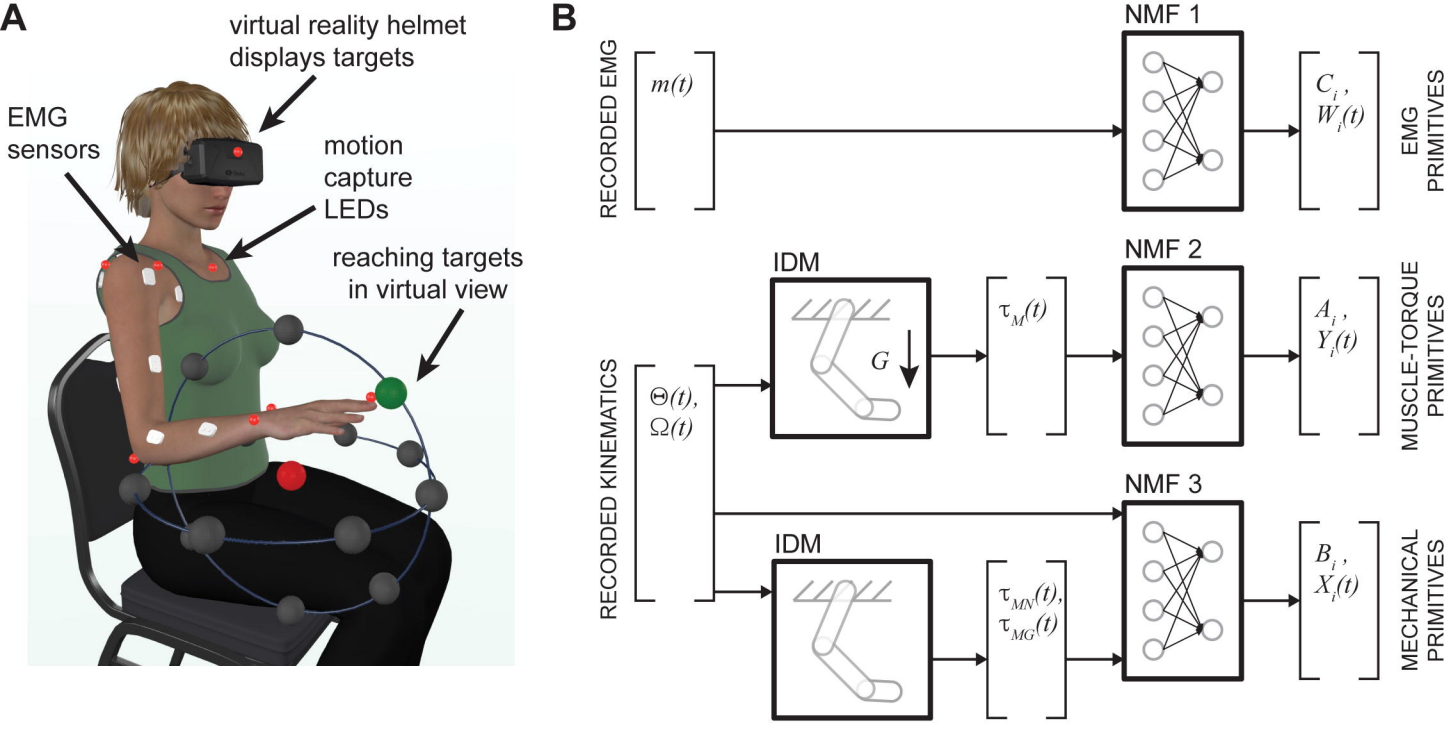
A
virtual reality helmet
displays targets
EMG
sensors
motion
capture
LEDs
reaching targets
in virtual view
B
RECORDED EMG
m(t)
NMF 1
C_i ,
W_i(t)
EMG
PRIMITIVES
IDM
G
τ_M(t)
NMF 2
A_i ,
Y_i(t)
MUSCLE-TORQUE
PRIMITIVES
RECORDED KINEMATICS
Θ(t),
Ω(t)
NMF 3
IDM
τ_MN(t),
τ_MG(t)
B_i ,
X_i(t)
MECHANICAL
PRIMITIVES

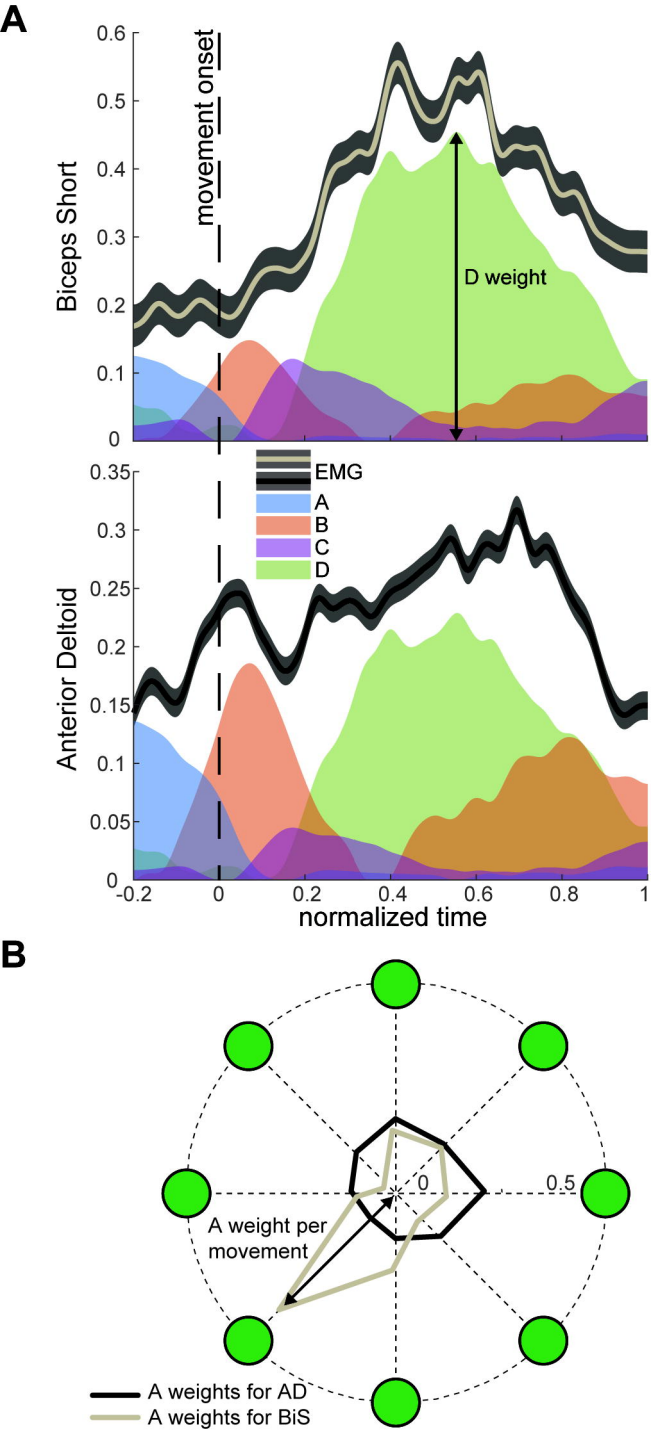
A
Biceps Short
movement onset
D weight
EMG
A
B
C
D
Anterior Deltoid
normalized time
B
A weight per
movement
0
0.5
A weights for AD
A weights for BiS

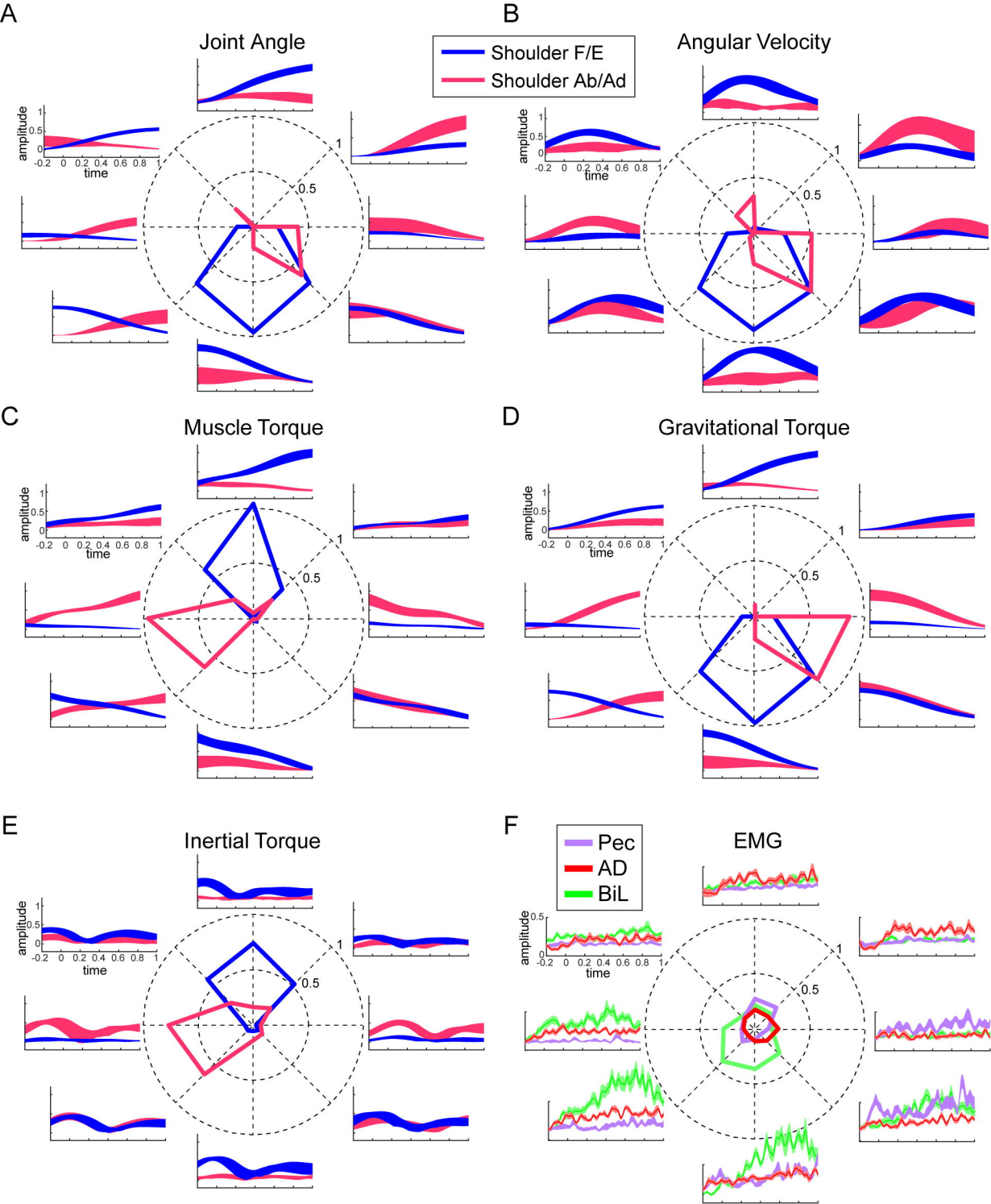
A
Joint Angle
B
Angular Velocity
Shoulder F/E
Shoulder Ab/Ad
C
Muscle Torque
D
Gravitational Torque
E
Inertial Torque
F
EMG
Pec
AD
BiL
amplitude
time
0.5
1

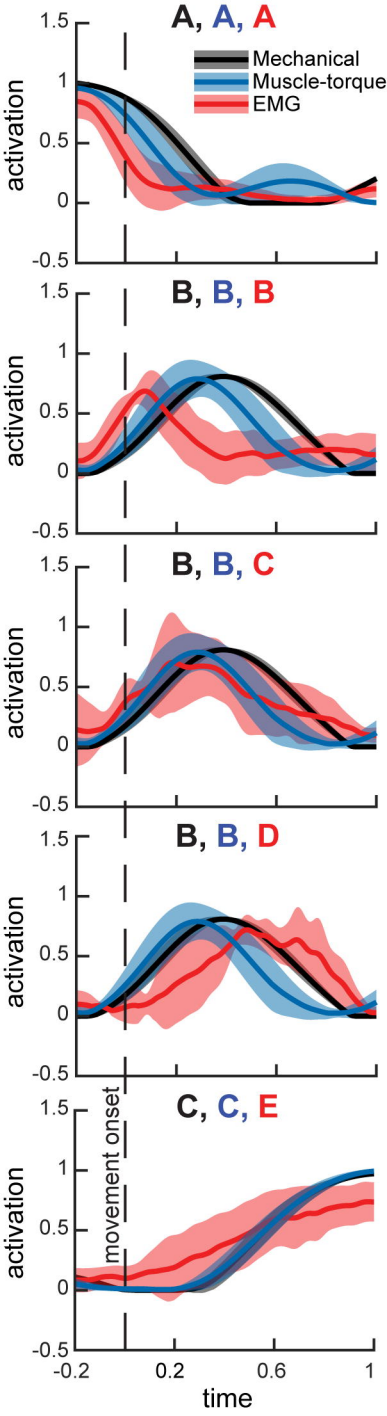
A, A, A
Mechanical
Muscle-torque
EMG
B, B, B
B, B, C
B, B, D
C, C, E
activation
movement onset
time
1.5
1
0.5
0
-0.5
-0.2
0.2
0.6
1

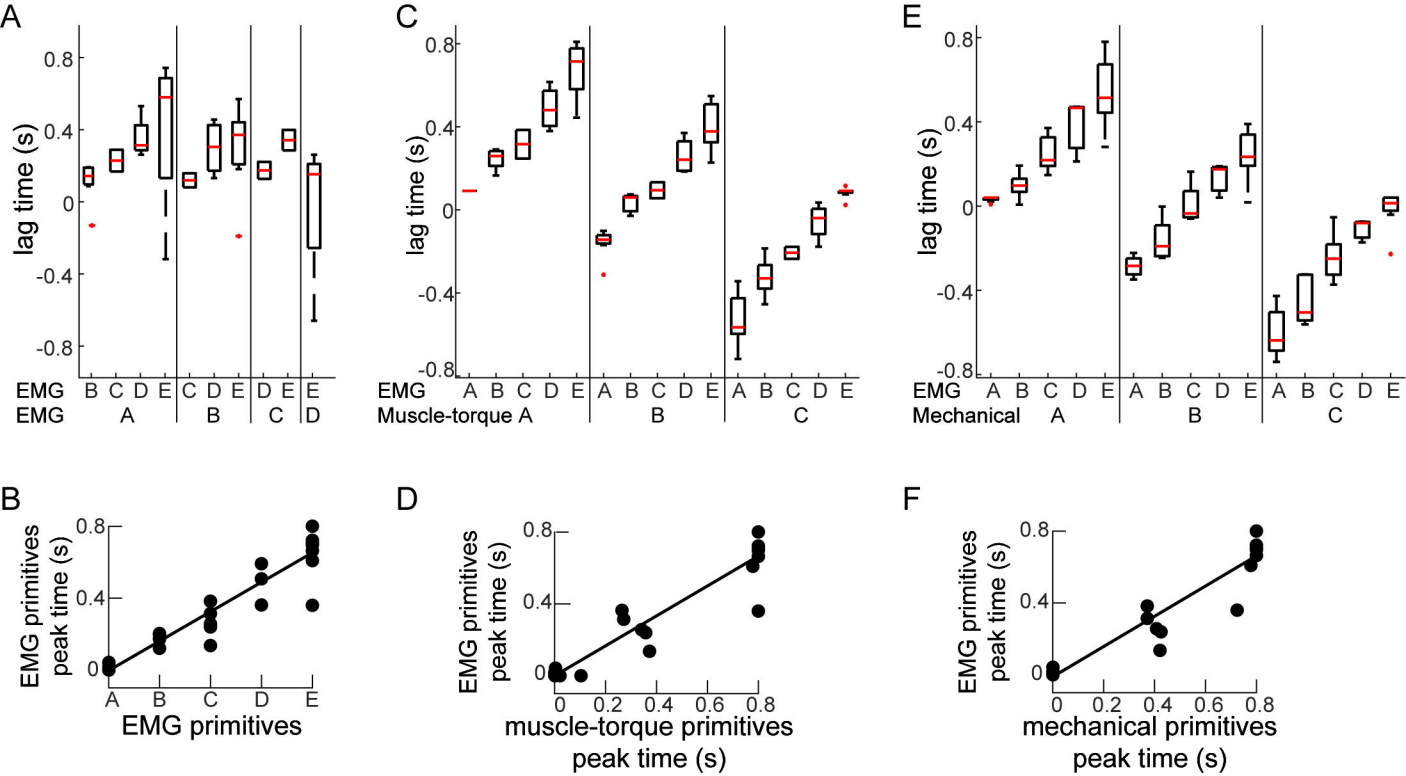
A
lag time (s)
0.8
0.4
0
-0.4
-0.8
EMG B C D E C D E D E E
EMG A B C D
C
lag time (s)
EMG A B C D E A B C D E A B C D E
Muscle-torque A B C
E
lag time (s)
EMG A B C D E A B C D E A B C D E
Mechanical A B C
B
EMG primitives peak time (s)
0.8
0.4
0
A B C D E
EMG primitives
D
EMG primitives peak time (s)
0 0.2 0.4 0.6 0.8
muscle-torque primitives peak time (s)
F
EMG primitives peak time (s)
0 0.2 0.4 0.6 0.8
mechanical primitives peak time (s)

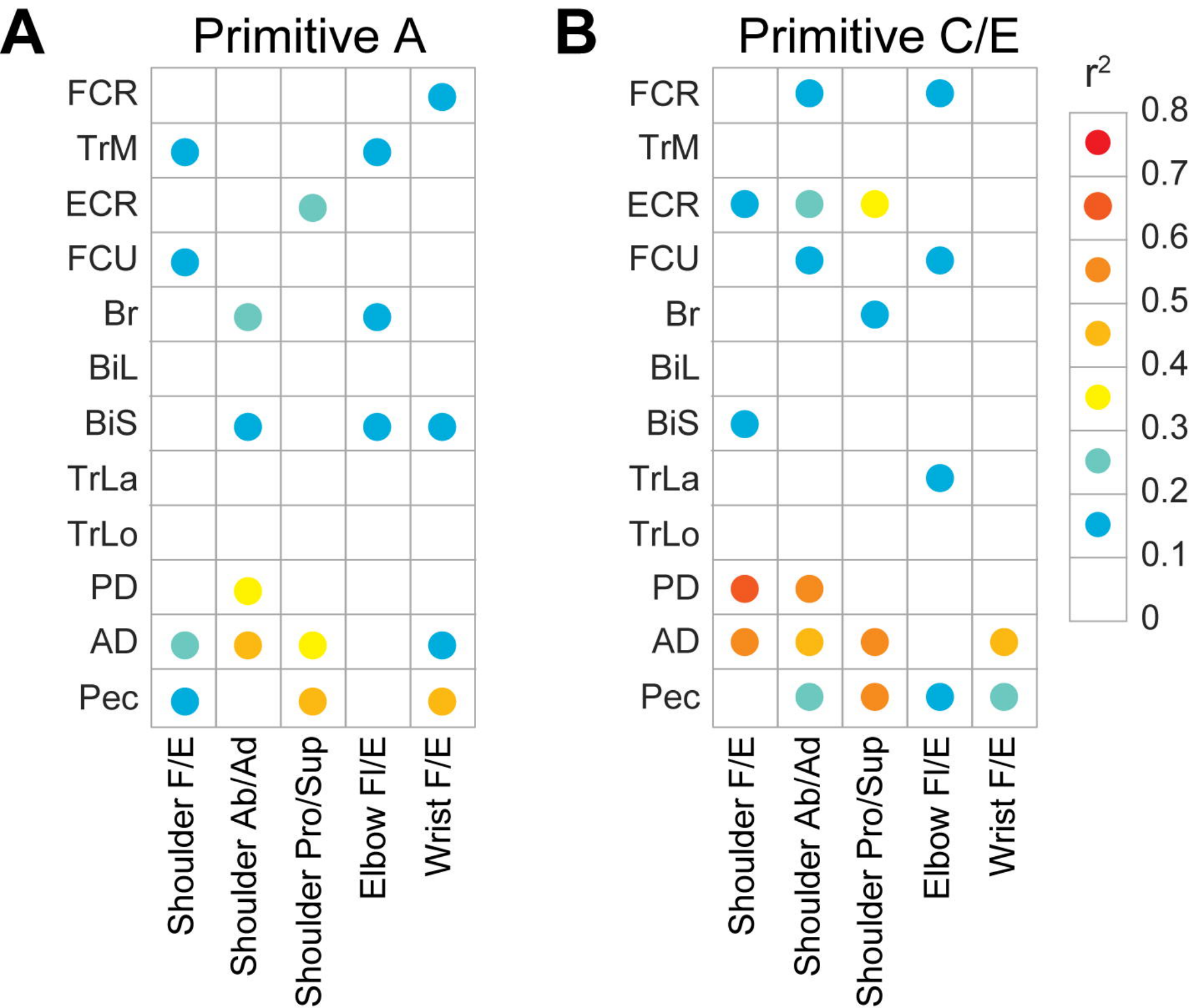
A
Primitive A
B
Primitive C/E
FCR
TrM
ECR
FCU
Br
BiL
BiS
TrLa
TrLo
PD
AD
Pec
Shoulder F/E
Shoulder Ab/Ad
Shoulder Pro/Sup
Elbow Fl/E
Wrist F/E
r2
0.8
0.7
0.6
0.5
0.4
0.3
0.2
0.1
0

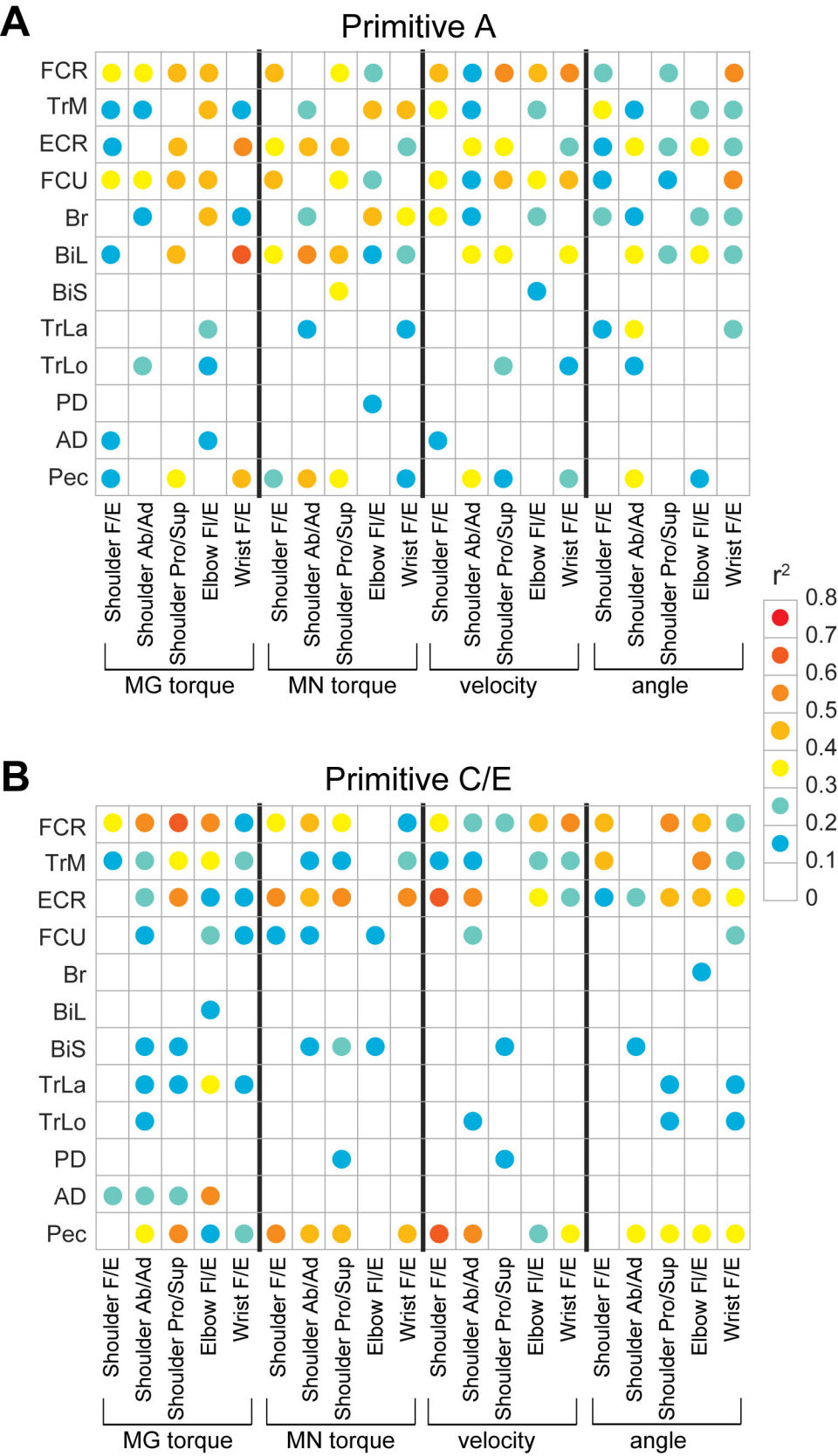
A
Primitive A
FCR
TrM
ECR
FCU
Br
BiL
BiS
TrLa
TrLo
PD
AD
Pec
Shoulder F/E
Shoulder Ab/Ad
Shoulder Pro/Sup
Elbow Fl/E
Wrist F/E
MG torque
MN torque
velocity
angle
r²
0.8
0.7
0.6
0.5
0.4
0.3
0.2
0.1
0
B
Primitive C/E